# Surface Potential and Local Conductivity Measurements of Micropatterned Aromatic Monolayers Covalently Attached to n-Si(111) via Si-C and Si-O bonds

Maria Carmela T. Garcia, Toru Utsunomiya, Takashi Ichii, and Hiroyuki Sugimura*

*Department of Materials Science and Engineering, Graduate School of Engineering, Kyoto University, Kyoto 606-8501, Japan*

E-mail: sugimura.hiroyuki.7m@kyoto-u.ac.jp

The surface potentials and local conductivity of self-assembled monolayers (SAMs) formed using aromatic molecules covalently bonded to n-type silicon (111) via Si-C and Si-O bonds were measured using Kelvin probe force microscopy (KPFM) and conductive AFM (CAFM). Surface potential measurements were done using micropatterned SAMs with hexadecyl SAM as reference to eliminate surface potential variations due to the cantilever tips. Micropatterning was conducted via vacuum ultraviolet (VUV) photolithography at $\lambda$ = 172 nm. Ellipsometry, X-ray photoelectron spectroscopy, static water contact angle and atomic force microscopy tests show that the aromatic SAMs were well-organized despite the short molecular lengths of the precursors. KPFM results show that Si-C bonded SAMs have higher surface potentials compared to Si-O SAMs, which is in agreement with dipole moments estimated by Molecular Orbital Package (MOPAC) semi-empirical computations. CAFM scans showed conductive domains for the aromatic SAM regions, and Si-O SAMs exhibited higher current than Si-C SAMs.

# 1. Introduction

The control of the chemical and physical properties of surfaces is a growing field in surface science and nanotechnology. One method to control surface properties for specific applications is through the use of self-assembled monolayers (SAMs), which are ultrathin 2D films composed of semirigid molecules chemically anchored to a substrate[1),2)]. Some applications of SAMs include friction control[3),4)], corrosion prevention[5),6)] and biosensing[7),8)], and recent studies have also probed its applications in molecular electronics[9)–13)] where they have been found to be helpful in improving charge injection between material interfaces.

Several studies have shown that organic molecules adsorbed on a substrate introduces a dipole moment to the surface[12),14),15)], which can easily be adjusted through the substitution of different functional groups[16)–18)]. This dipole layer at the surface constructs a potential shift, leading to changing the substrate work function[19),20)] and improving the efficiency of charge carrier injection in electronic devices[15),21)]. In addition to the intrinsic dipole moment of the precursor molecule, a change in the work function or surface potential may be affected by the docking chemistry of the SAM[16),22)], packing of the molecules[23)] and depolarization between neighboring molecules[24)]. While the intrinsic dipole moment of the precursor molecule can provide initial insight on the resulting surface potential, the chemical bonding of the adsorbate to the substrate often results in charge rearrangements at the interface, which can lead to differences between the dipole of the precursor molecule and the dipole of the SAM itself[16)]. In this case, the contributions to the net dipole moment of the SAM depend on the strength of the interaction between the molecule and substrate[16),22)] and the polarizability of the molecule backbone[25)].

Although many studies have focused on thiol SAMs on metal substrates such as gold and silver[12),15),26)–29)], recently the use of semiconductor substrates has been attracting interest[16),23),30)–32)]. Due to their more complex energy band systems, the effects of SAMs on the work function of semiconductors can be affected by several factors such as band bending, and doping level and type, which requires more in depth studies to be fully understood[33)–36)]. Semiconductors have many applications in electronic devices and understanding how certain modifications can tune its device characteristics can help advance modern technology. Among semiconductors, silicon has been attracting much attention due to its wide use in present electronics[32)]. The study of interfaces between silicon and organic materials plays an important role in emerging research fields such as molecular electronics and biotechnology.

SAMs can be grafted on silicon in several ways. Many studies have used silanes where an oxide layer exists between the silicon substrate and the adsorbate[3),37),38)]. In molecular electronics, these types of SAMs are often used as electrical insulators or dielectrics[39),40)], where the thickness can easily be controlled through the molecular length of the precursor molecule. Direct attachment of the molecule to the silicon substrate is also possible through covalent bonds such as Si-C[41)–44)], Si-O[41),42),45)], Si-S[41),46)], Si-N[41),45)] and Si-Te[46)]. The chemical bond between silicon and the SAM molecule is known to affect the energy levels of the molecular orbitals which can affect the surface potential of the substrate, as well as the conduction through the molecule[16),22),45),47),48)]. Alkyl-SAMs grafted directly to the silicon substrate with Si-C bonds display high chemical resistivity[42),49),50)]. Grafting the molecules directly to silicon without the intermediate oxide layer can provide electrical connections between the SAM and substrate[51)]. The saturated σ bonds in the molecule result in the SAMs with low conductivity, and thus they are capable of sustaining high electric fields before breakdown[52)]. When unsaturated bonds are present in the precursor molecules, such as in the case of aromatic molecules, other electrical properties of silicon may be achieved[47),53),54)]. Similar to surface potential, the electronic properties, such as conductivity, of the surface may be affected by SAM parameters including the molecule-substrate bond[47)].

In this study we investigated the effects of Si-C and Si-O bonding of aromatic SAMs attached directly to silicon on the surface potential and conductive properties. We have chosen to use styrene ($C_6H_5CH=CH_2$), 4-phenyl-1-butene ($C_6H_5(CH_2)_2CH=CH_2$), benzyl alcohol ($C_6H_5CH_2$-OH), and 3-phenyl-1-propanol ($C_6H_5(CH_2)_3$-OH) as our aromatic precursors. Measurements of the surface potential of SAMs were conducted using Kelvin Probe Force Microscopy (KPFM). This method allows us to map the local surface potential distribution of the sample surface simultaneously with its topography. Conductive AFM (CAFM) was used to measure the current passing through the SAMs. To account for any variations that may occur during KPFM and CAFM measurements due to changes in the cantilever tips, micropatterned SAMs were used with 1-hexadecene ($CH_3(CH_2)_{13}CH=CH_2$) SAM acting as the reference. Due to the Si-C bond of the SAM, which is resistive to HF etching, it has shown to be suitable for use as a photoresist and reference SAM in our past KPFM measurements[22),55)].

# 2. Experimental methods

## 2.1 Materials

The substrates were phosphorus doped n-type Silicon (111) wafer with resistivity range of 1-10 Ω cm from Electronics and Materials Corp. Styrene (>99%, stabilized with TBC), benzyl alcohol (>99%), 4-phenyl-1-butene (>98%), and 3-phenyl-1-propanol (>98%) were purchased from Tokyo Chemical Industry and were used as the SAM precursors. Ethanol (99.5%), and mesitylene (98%) were purchased from Nacalai Tesque. Hydrofluoric acid (HF) and ammonium fluoride ($NH_4F$) for the hydrogen termination were purchased from Morita Chemical. All chemicals were used as received and without further purification.

## 2.2 Sample Preparation

The method for the preparation of the micropatterned SAMs are shown in Fig. 1. Si(111) wafers were cut into 1 × 1 $cm^2$ before being ultrasonically cleaned in ethanol and ultrapure water (UPW) for 20 minutes each. This was followed by photochemical cleaning in ambient environment using vacuum ultraviolet (VUV) light from a Xe-excimer lamp source (UER 20-172V, Ushio) to remove organic contaminants on the surface of the wafer. Hydrogen-terminated silicon (H-Si, Fig. 1a) was prepared by etching the substrate in a 5% HF solution for 5 minutes in the dark, followed by immersion in a 40% $NH_4F$ solution for 60 seconds. The $NH_4F$ solution was heated to 80°C prior to the substrate immersion to eliminate the dissolved oxygen, which may result in the etch pits on the substrate.

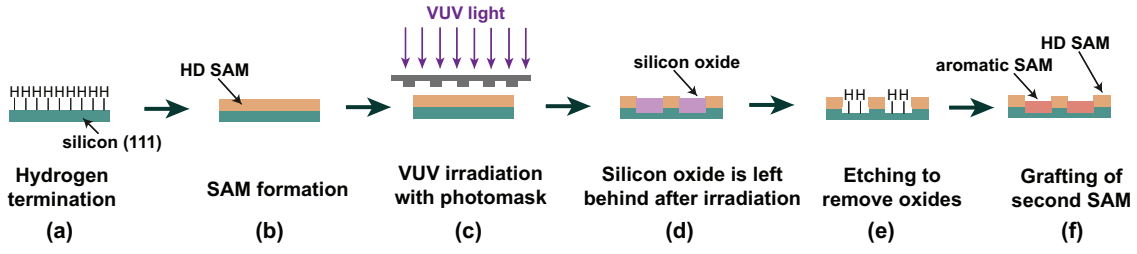


**Fig. 1.** Schematic illustrations for forming the micropatterned SAMs using VUV photolithography

The reference SAM in this study was formed using neat 1-hexadecene (HD) as a precursor and will be referred to as HD SAM in this paper (Fig. 1b). The H-Si substrate was first placed in a custom-made quartz vessel which consisted of a rectangular quartz cell (5 mm thickness) attached to a cylindrical tube with a volume of about 100 $cm^3$. The H-Si substrate and 1-

hexadecene precursor were placed inside the vessel and irradiated with UV light (high pressure Hg lamp, REX-250, $\lambda$ = 240 - 440 nm, Asahi spectra) for 1 hour at the intensity of 100 mW $cm^{-2}$. To minimize any unwanted oxidation of the silicon substrate, the vessel was purged with $N_2$ gas at least 30 minutes prior to irradiation, and the gas continued to flow for the entire irradiation process. After irradiation, the substrate was removed from the vessel and ultrasonically cleaned using ethanol and UPW for 10 minutes each to remove any physisorbed molecules on the surface. The resulting SAM formed on the silicon substrate was used as the reference material for all KPFM in this paper.

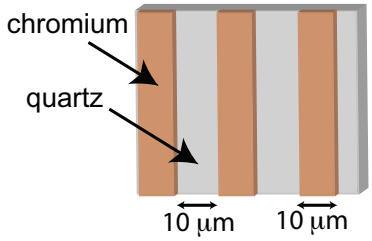


**Fig. 2**. Schematic illustration of photomask used during VUV irradiation

The HD SAM underwent micropatterning via VUV photolithography with a Xe-excimer lamp (UER20-172V, Ushio) with a wavelength of 172 nm and intensity of 10 mW $cm^{-2}$. Figure 1c shows the schematic of the micropatterning process. A photomask consisting of 100 nm thick chromium pattern attached to a 2 mm thick quartz plate, whose transparency at $\lambda$ = 172 nm was 93%, was used to cover regions of the HD SAM while allowing VUV light to irradiate the uncovered regions (Fig. 2). The sample was placed in the VUV irradiation chamber at a distance of 5 mm from the lamp window. The pressure inside the chamber was kept at ~$10^3$ Pa and the sample was irradiated for 30 minutes. Photo- excitation by the VUV light irradiation converted the oxygen molecules inside the chamber to a more reactive singlet and triplet states (O(1D) and O(3P)). This excited oxygen degraded the uncovered monolayer and left the region to contain silicon oxide (Fig. 1d). The silicon oxide was removed through another round of HF and $NH_4F$ etching for the hydrogen termination (Fig. 1e), allowing a new SAM to be grafted in the irradiated place. Although the etching process after VUV photolithography was very similar to the one described above, the etching time in HF was shortened from 5 min. to 3 min., and etching time in $NH_4F$ was shortened from 60 s to 45 s to minimize the damage on the remaining HD SAM. After the etching, a new SAM was attached to the H-Si regions using the same method described earlier (Fig. 1f). The precursors to form the SAMs were styrene (1 M solution), benzyl alcohol (neat), 4-

phenyl-1-butene (1 M solution), and 3-phenyl-1-propanol (2 M solution). The solvent for these precursor solutions was mesitylene. The SAMs in the study will be referred to as Styrene SAM (styrene), BA SAM (benzyl alcohol), 4P1B SAM (4-phenyl-1-butene), and 3P1P SAM (3-phenyl-1-propanol). The diagram of the SAMs grafted to silicon is shown in Fig. 3. Two of the SAMs (styrene SAM and 4P1B SAM) are grafted to silicon via a Si-C bond while the other two (BA SAM and 3P1P SAM) are grafted via a Si-O bond. The SAMs were also individually investigated to determine its quality using X-ray photoelectron spectroscopy (XPS, ESCA-3400 Kratos Analytical), static contact angle meter (DM 500, Kyowa Interface Science CA-X Co.), atomic force microscopy (AFM, MFP-3D, Oxford Instruments), and ellipsometry (FE-5000, Otsuka Electronics).

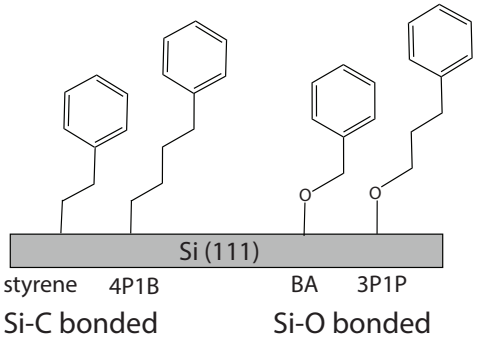


**Fig. 3.** Diagram of the molecules grafted on Si substrate via Si-C and Si-O bonds

Kelvin Probe Force Microscopy (KPFM) based on amplitude modulation (AM) AFM was used to map the topography and surface potential contrasts of the micropatterned SAMs using a two-pass procedure. The topographic line was acquired first using AM mode while the surface potential measurements were acquired afterwards using lift mode. Measurements were conducted in ambient environment with a Rh-coated silicon cantilever tip (SI-DF-3R, Hitachi Hitech). The cantilever resonance frequency was approximately 27 kHz. The AC bias voltage with an amplitude of 1.0 V was added between the sample and the tip at around the same frequency as the cantilever. The scanning probe rates were ranged from 0.5 to 0.8 Hz. To ensure reliability of data, a minimum of 3 samples for each system was prepared and at least 3 measurements were taken at different positions on the sample surface. Since KPFM measurements may be affected by contaminants or adsorbed water on the surface, samples were analyzed immediately upon preparation to minimize these effects[56)–58)].

To observe the electrical conductivity of the SAMs, the samples were scanned using conductive atomic force microscopy (CAFM) based on contact-mode AFM. A Rh-coated silicon cantilever tip (SI-DF-3R, Hitachi Hitech) with a spring constant of 1.6 N $m^{-1}$ was used. A transimpedance amplifier with an 82 MΩ feedback resistor was used to convert the

current signal to the voltage. The tip load was kept at 4.35 nN. A -1.0 V bias was applied to the tip relative to the grounded silicon substrate.

## 3. Results and discussion

*Formation of aromatic SAMs*

First, we describe the result on single-component SAMs. Since surface potential measurements are very sensitive to the SAM quality, ensuring the quality of our SAMs is important before KPFM measurements. Table I shows the water contact angles (WCA), ellipsometric thicknesses and atomic concentrations of the SAMs formed for this study. The values reported for these measurements are the average of multiple samples with their statistical errors. The atomic concentration was measured by XPS. The properties of H-Si are also shown for comparison. The H-Si substrate has a WCA of about 85.5 degrees. After the HD SAM formation, this increased significantly to 106.0 degrees, suggesting that the surface consisted of a dense methyl-terminated surface[42),59),60)]. For the Si-C bonded SAMs (styrene and 4P1B), the WCA was about 85 degrees, while for the Si-O bonded SAMs (BA and 3P1P) it was about 82 to 83 degrees. These WCA values were much smaller than HD SAM's and were close to the H-Si value. However, they are close to the expected value obtained by Popoff on their phenyl terminated SAM formed on oxide-free silicon (between 80 to 81 degrees)[61)]. The phenyl headgroup is much less hydrophobic than the methyl headgroup, which results in a lower WCA[62)]. Since the WCA of the aromatic SAMs were very close to that of H-Si, it is difficult to conclude if the molecule was grafted based on this test alone, thus XPS analysis was conducted.

The atomic concentration of H-Si and the SAMs are shown in Table 1, while Fig. 4 shows the C 1s, O 1s and Si 2p peaks obtained from XPS analysis. The binding energies and intensities were referenced and normalized to the Si 2p peak of bulk silicon at 99.5 eV. The C 1s peak of all SAMs shows a substantial increase compared to H-Si suggesting that the precursor molecules were successfully grafted on to the substrate. The C 1s atomic concentrations of the aromatic SAMs were much less than that of HD SAM, because the precursor molecules itself consist of less carbon atoms. A study by Harada et al. found that despite the difference in molecular structure, long alkyl SAMs and aromatic SAMs experience similar limitations when it comes to surface coverage[47)]. Highly ordered SAMs are characterized by dense packing of the molecules on the surface, due to strong

intermolecular interactions in the film, as seen in Fig. 5. For alkane SAMs, strong Van der Waals forces are present between chains, which allows them to pack densely on the surface. This was confirmed by the high water contact angle of our HD SAM due to the dense methyl terminated surface[42),59),60)]. For phenyl monolayers, it is thought that the primary intermolecular force between molecules is the π–π stacking of the phenyl rings, which also results in a dense and ordered monolayer.

Our XPS results show that the carbon concentration increased from 5.4% (for H-Si) to about 20-24% (for Si-C bonded SAMs) and 17-19% (for Si-O bonded SAMs), indicating the presence of an organic film on the surface. The higher carbon concentration of the Si-C SAMs compared to the Si-O SAMs may be due to the presence of more molecules grafted to the surface as a result of greater packing, or may simply be due to the additional carbon atom in the molecular precursor. Nevertheless, the increase in carbon concentration of the SAMs compared to the H-Si sample suggest that the precursor molecules were successfully grafted to the substrate and that the SAMs were formed with 1 hour of UV irradiation. The Si 2p spectra of all the SAMs show a single peak centered at 99.5 eV, with no peak present at 103 eV, indicating that the underlying Si substrates were well passivated with the precursor molecules (Fig. 3). The O 1s concentration for the Si-O bonded SAMs was higher than the Si-C bonded SAMs, which is expected due to the -OH group present in the head group of the SAM precursor. The presence of the O 1s peak in all the SAMs suggests that although the substrate was passivated and no peak at 103 eV was present, trace amounts of silicon oxide might be present. A spectroscopic study on aromatic SAMs on Si(111) found that the trace oxidation detected by XPS originated from oxidation of the silicon surface during the SAM growth and not from contamination or oxidation of the sample as it was loaded to the UHV XPS chamber[47)]. Complete inhibition of the oxidation of the silicon substrate was not achievable due to the 50% molecular packing of the aromatic SAMs that has been reported in several literature[45),47),53)]. This amount of coverage for aromatic SAMs is considered densely packed.

**Table I.** Water contact angle (WCA), ellipsometric thickness and XPS atomic concentration of formed SAMs

| Sample | WCA (°) | Ellipsometric thickness (nm) | XPS Atomic Concentration | | | Precursor molecule length (Å) |
|---|---|---|---|---|---|---|
| | | | C 1s (%) | O 1s (%) | Si 2p (%) | |
| H-Si | 85.5 ± 1.8 | 1.49 ± 0.1 | 5.4 ± 0.8 | 3.2 ± 0.3 | 91.4 ± 1.1 | - |
| HD SAM | 106.0 ± 1.8 | 2.53 ± 0.24 | 33.5 ± 2.4 | 6.3 ± 1.2 | 60.2 ± 3.0 | 20.59 |
| Si-C bonded SAM | | | | | | |
| Styrene SAM | 85.4 ± 0.8 | 2.05 ± 0.02 | 20.8 ± 1.3 | 3.6 ± 1.3 | 75.5 ± 0.3 | 7.29 |
| 4P1B SAM | 84.7 ± 0.7 | 2.10 ± 0.18 | 23.9 ± 1.0 | 5.0 ± 1.2 | 71.1 ± 2.1 | 9.46 |
| Si-O bonded SAM | | | | | | |
| BA SAM | 82.0 ± 0.6 | 1.92 ± 0.11 | 17.5 ± 2.1 | 5.0 ± 2.1 | 77.5 ± 2.7 | 7.17 |
| 3P1P SAM | 82.5 ± 2.1 | 1.99 ± 0.04 | 18.3 ± 0.4 | 7.5 ± 0.5 | 74.2 ± 0.9 | 9.20 |

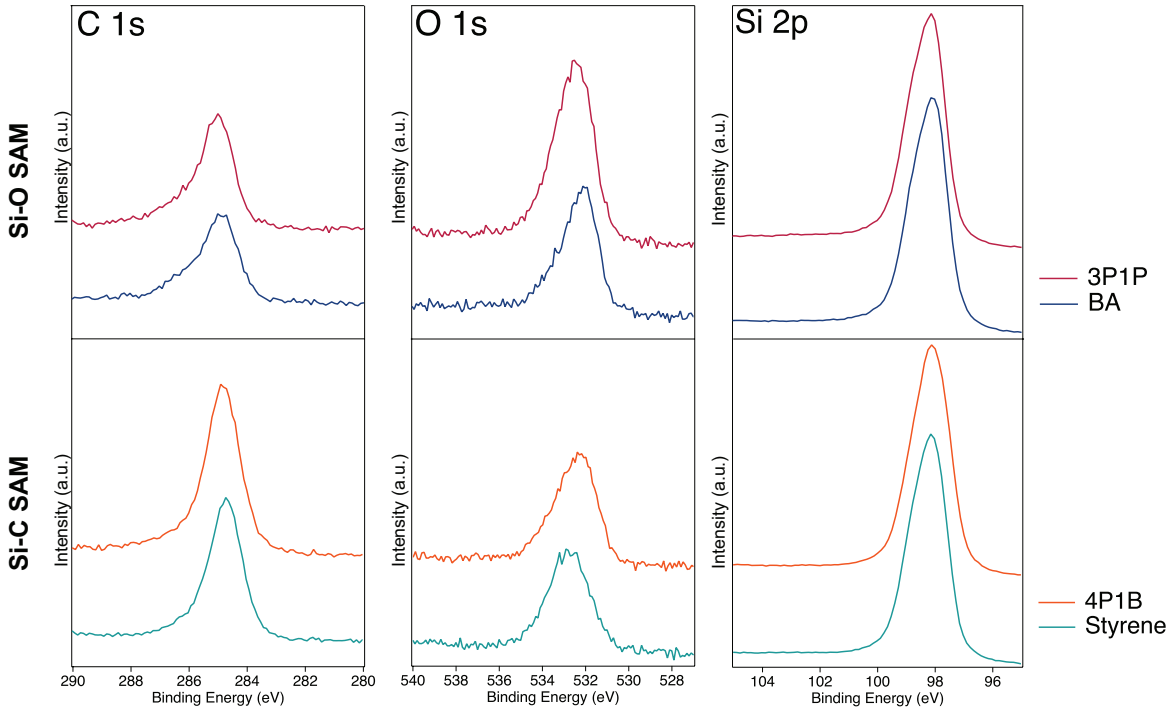


**Fig. 4.** XPS spectra of the Si-O and Si-C bonded SAMs obtained from each precursor.

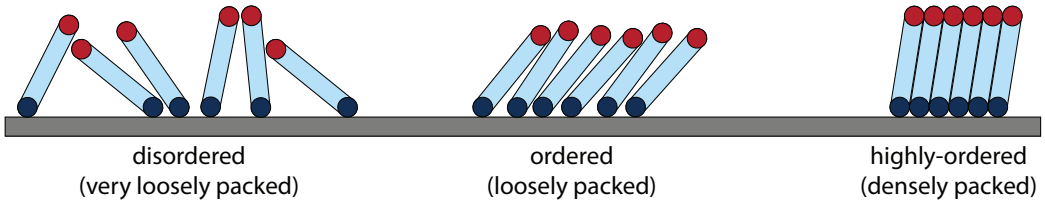


**Fig. 5.** Possible packing arrangements of molecules in SAMs

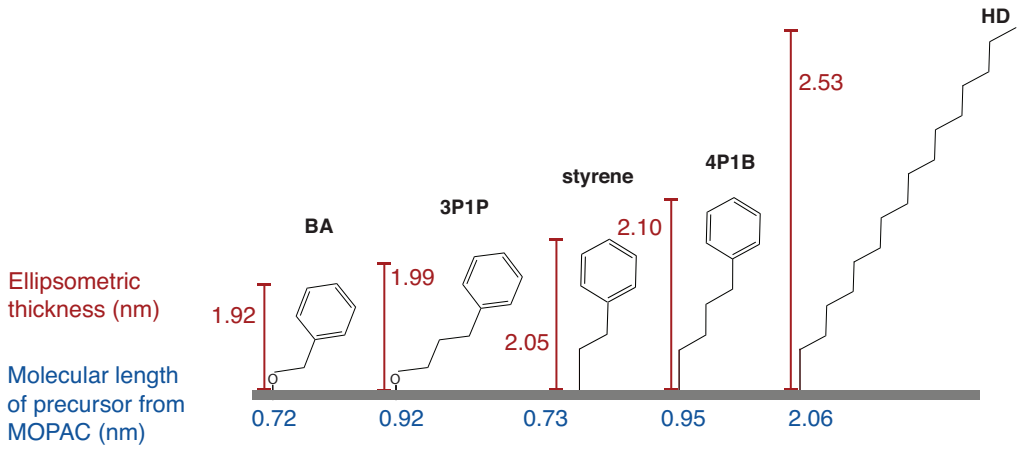


**Fig. 6**. Ellipsometric thickness of SAMs with MOPAC molecular length of precursors

The thickness of the SAMs was measured using ellipsometry. It should be noted that thickness measurements using ellipsometry often come with uncertainties due to the unknown refractive index of the SAM. However it provides a good basis for comparison between samples. The ellipsometric measurements showed that HD SAM had a thickness of 2.53 nm. The thicknesses of the aromatic SAMs were lower – about 2.05-2.10 nm for the Si-C bonded SAMs, and 1.92-1.99 nm for the Si-O bonded SAMs. This is expected since the precursor molecule for HD SAM has a long hydrocarbon chain that form straight up from the surface as opposed to that of the aromatic SAMs which consists of a benzene ring and a short methyl chain (about 1-2 units long). The increased thickness of the samples from H-Si suggests that the SAMs were successfully grafted to the substrate. The ellipsometry results showed that the Si-C bonded SAMs were slightly thicker than the Si-O bonded SAMs. This is in agreement with the estimated molecular length of our precursor molecules from our MOPAC semi-empirical computations (Table I). Additionally, the reported bond length of Si-C (1.90 Å) is slightly longer than that of Si-O (1.64 Å)[63]. The computed molecular length and reported bond lengths of Si-C and Si-O are in agreement with our ellipsometry measurements where Si-C SAM was slightly thicker than Si-O SAM. However the difference in the estimated molecular length between the Si-C and Si-O precursors with the

same amount of methylene spacer (styrene/BA and 4P1B/3P1P) is very small and the ellipsometry measurements gave a more noticeable difference (Fig. 6). Combined with the lower WCA of the Si-O SAMs, these results might suggest that the molecules for Si-O SAMs were slightly more tilted than the Si-C SAM, possibly due to lower molecular density. Previous studies on Si-C bonded alkyl-phenyl molecules suggested that the more tilted molecules resulted in a lower WCA[45),53)] The more vertically-oriented molecules displayed greater hydrophobicity due to the increased exposure of the C-H bonds, as opposed to the tilted molecules that had the phenyl ring more inclined. It is possible that the Si-O SAMs experienced more tilting compared to the Si-C SAMs due to the difference in their packing densities, as shown in our diagram in Fig 6.

The topography of the SAMs was observed using AM-AFM. Figure 7 shows AFM images of the SAMs surface. Clear terraces and atomic steps were observed for all samples. The step height for all samples were measured to be around 0.3 nm, which is in agreement with the theoretical 0.31 nm value of monoatomic steps on Si (111) surfaces[64)]. This suggests that all SAMs formed uniformly on the H-Si substrate.

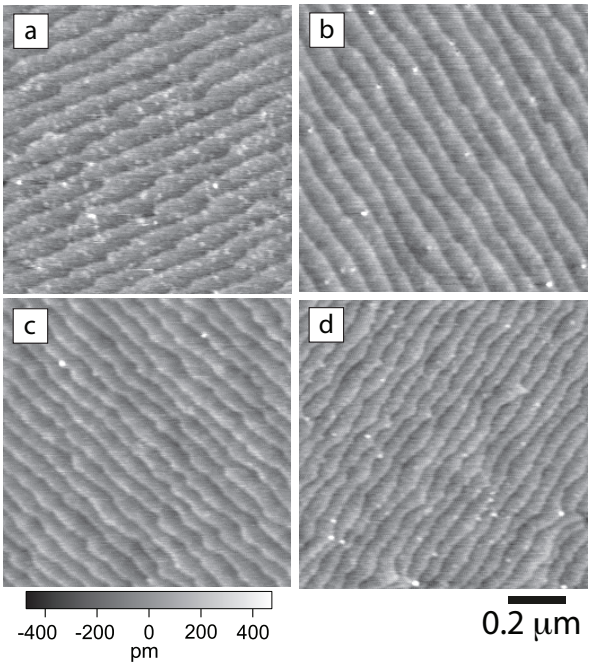


**Fig. 7.** AFM images of the terrace step structure of (a) styrene SAM, (b) 4P1B SAM, (c) BA SAM and (d) 3P1P SAM

From the XPS, AFM, WCA and ellipsometry results, it can be concluded that these aromatic molecules formed highly-ordered monolayers on n-Si(111) despite the short alkyl

chain length and the bulky phenyl group. Although short-chained monolayers have been found to form disordered SAMs, in our study the SAMs exhibited high-order even with the short chains, which can be attributed to the π−π stacking of the aromatic rings[53].

Individual characterization of all the SAMs in this study showed that they were formed uniformly with minimal oxidation of the silicon substrate. This is crucial since even slight oxidation of the underlying silicon substrate can heavily affect the KPFM measurements[55] as well as conduction through the monolayer[47),65]. As such, it is possible to proceed with KPFM analysis and CAFM using the SAMs formed above.

*Surface Potential Measurements*

From here we will discuss the results on the micro-patterned SAMs. The surface potential of aromatic SAMs was measured against HD SAM using KPFM analysis. Figure 8 shows the topography and surface potential images of the samples and the results are summarized in Table II. The topography and surface potential values reported here are the average of several samples with their statistical errors. For the topography measurements, the higher regions (brighter) correspond to the reference HD SAM while the lower regions (darker) correspond to the aromatic SAMs. Ellipsometry measurements in Table I have shown that all the aromatic SAMs had a lower thickness than the reference HD SAM, which was confirmed in our KPFM/AFM results. Additionally, the aromatic SAMs which were grafted after the VUV photolithography and etching were attached to regions of the substrate which had been lowered due to etching (Fig. 1f). Thus, the reference HD SAM has a higher topography than any of the aromatic SAMs used in this study. Our previous experiments have shown that the VUV photolithography process and the etching lowers the topography of the irradiated silicon substrate by about 1.38 nm[55].

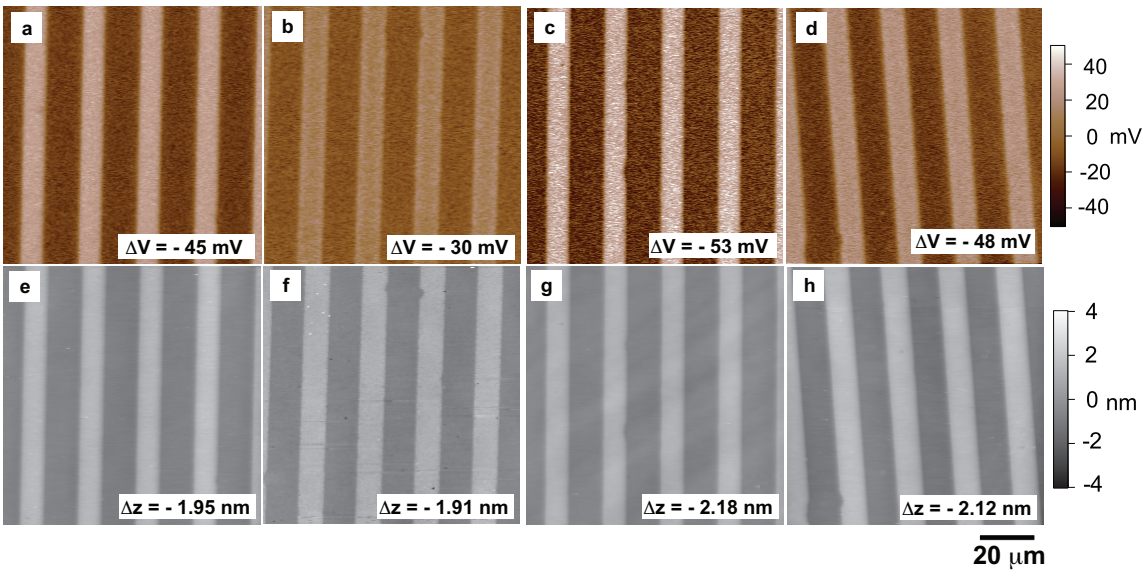


**Fig. 8.** Simultaneously obtained (a-d) surface potential and (e-h) AFM height images of the micropatterned samples, corresponding to (a,e) styrene SAM, (b,f) 4P1B SAM, (c,g) BA SAM, and (d,h) 3P1P SAM. We used HD SAM as a reference for all samples.

Our previous research has also shown that after the micropatterning process, the surface potential of the newly-deposited HD SAM was lower than that of the reference HD SAM by 15.3 mV[55]. This is most likely due to the damage that occurs on the reference HD region during the etching process. Figure 9 shows the topographic images obtained on the newly-deposited aromatic SAM region and the reference HD SAM region. The HD SAM region sustained some damage due to the etching process, which is seen as etch pits. This resulted in an increase in the surface potential of the reference HD region due to oxidation in the area and/or the slight degradation of the SAM. However, this increase was reproducible and consistent during our experiments and the data is still reliable.

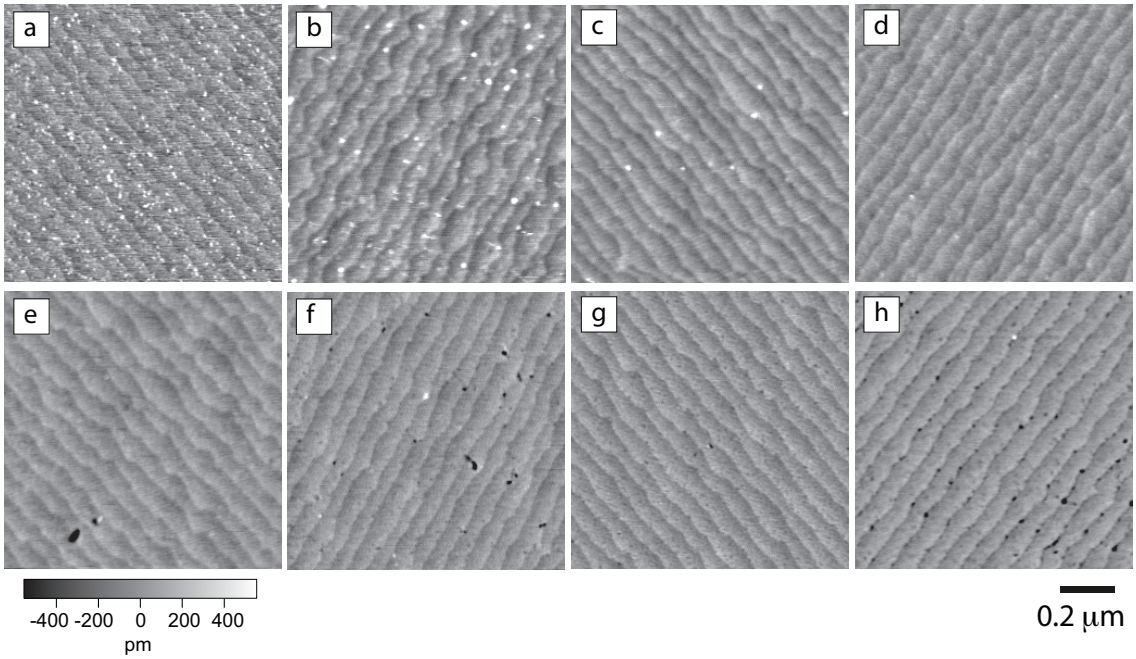


**Fig. 9**. AFM images of aromatic SAMs (a-d) and reference HD SAM (e-h) regions of the micropatterned surfaces, corresponding to (a,e) HD-styrene, (b,f) HD-4P1B, (c,g) HD-BA, and (d,h) HD-3P1P. The corresponding HD SAM reference regions (e-h) exhibit damage in the form of etch pits.

**Table II.** Surface potential and topography contrast of micropatterned SAMs

| | Surface potential contrast (mV) | Topography contrast (nm) |
|---|---|---|
| HD-HD | -15.3 ± 1.8 | -1.38 ± 0.09 |
| Si-C bonded | | |
| HD-Styrene | -45.2 ± 7.1 | -1.95 ± 0.10 |
| HD-4P1B | -30.3 ± 1.0 | -1.91 ± 0.07 |
| Si-O bonded | | |
| HD-BA | -52.5 ± 6.6 | -2.18 ± 0.30 |
| HD-3P1P | -47.5 ± 3.3 | -2.12 ± 0.25 |

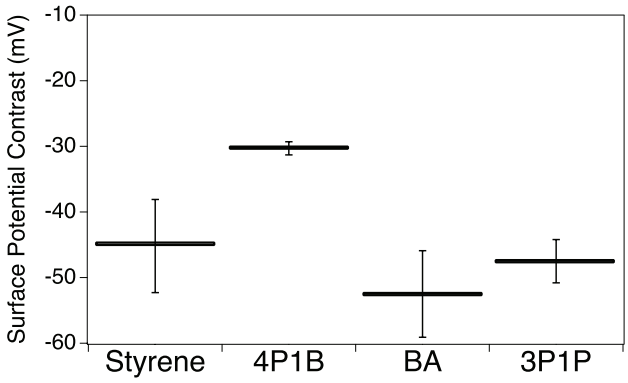


**Fig. 10**. Surface potential contrasts of the SAM with respect to reference HD SAM

In the KPFM measurement, the surface potential difference was measured to be -45.2 mV, -30.3 mV, –52.5 mV and -47.5 mV for styrene SAM, 4P1B SAM, BA SAM and 3P1P SAM respectively (Fig. 10). Taking the damage exhibited on the reference HD SAM into consideration, this tells us that the actual contrast from HD SAM was -29.9 mV, -15.0 mV, -37.2 mV and -32.2 mV for styrene SAM, 4P1B SAM, BA SAM and 3P1P SAM respectively. The surface potential of a SAM is affected by the dipole moment of the molecules grafted on the surface, the molecular packing and the dielectric constant of the SAM. The surface potential difference between a tip and a SAM is given by Eq. (1), where the terms $\phi_{Si}$ and $\phi_{tip}$ correspond to the work functions of the silicon substrate and the tip, and $e$ is the electric charge[18),66),67)]. In the second term, $\mu$ is the net dipole perpendicular to the surface, $A$ is the area occupied by the molecule, $\epsilon_0$ is the permittivity of free space and $\epsilon_{SAM}$ is the relative permittivity or dielectric constant of the SAM. Since the two SAMs are deposited on the same silicon substrate, the difference in surface potentials can be obtained using Eq. (2) where $V_{\mathrm{SAM}}$ and $V_{\mathrm{SAM(HD)}}$ are the surface potentials of the aromatic SAM and reference HD SAM respectively.

$$V_{SAM} = -\frac{\phi_{Si}-\phi_{tip}}{e} + \frac{\mu}{A\epsilon_0\epsilon_{SAM}} \quad (1)$$

$$V_{SAM} - V_{SAM(HD)} = \frac{\mu_{SAM}}{A_{SAM}\epsilon_0\epsilon_{SAM}} - \frac{\mu_{SAM(HD)}}{A_{SAM(HD)}\epsilon_0\epsilon_{SAM(HD)}} \quad (2)$$

In the Eq. 1, $\mu$ represents the net dipole moment of the SAM that is normal to the substrate[67)]. In previous studies where molecules were attached to the substrate via the same bond, researchers used simplified molecule computations to obtain $\mu$, without considering the interfacial dipole moment[17),31),67)]. This is because the interfacial dipole moment was

assumed to be constant for all SAMs due to the identical binding group, and thus any difference in surface potential would be a result of the remaining part of the molecule. However, in our study it is clear that the effect of the different binding groups played a significant role. The dipole moment of the aromatic SAMs was computed using MOPAC semi-empirical computations (Fig. 11-12). In Fig. 11, the dipole moments of only the precursor molecules were considered, while in Fig. 12 the molecules are grafted to a silicon atom, as they would be once the SAM has attached to the substrate. It should be noted that these are semi-empirical computations using only one silicon atom instead of a silicon slab consisting of several layers, which is usually used in papers doing computational analysis[16),30),45)]. However, they would provide a general estimate of the dipole moments for comparison with each other. It is clear that the binding of the molecules to the substrate result in some charge rearrangement in the molecular backbone which alter its dipole moment. The nature of the bond is thus quite significant in the final dipole moment of the SAM when it is grafted to the substrate. The dipole computations including the attachment to a silicon atom agree qualitatively with the results of our KPFM measurements under the assumption that the precursors were perpendicularly bound to the Si substrate.

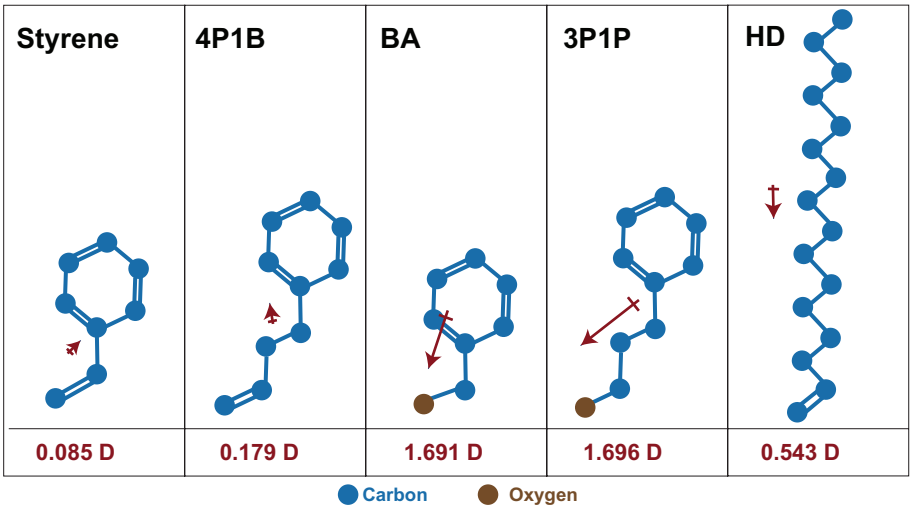


**Fig. 11.** Dipole moments of precursor molecules computed via MOPAC. Arrowhead points to the negative end of the dipole.

The dipole moments of all the SAMs have the positive pole pointing away from the surface after grafting, as shown in Fig. 12. This direction increases the potential at the surface and decreases the electron affinity and work function. This can be imagined as an electron from the conduction band of the surface being accelerated by the dipole to the local vacuum,

making it easier for the electron to break free[36]. On the other hand, a dipole of the opposite direction will decrease the surface potential, while increasing the electron affinity and work function, due to the additional barrier to the electron to escape from the surface. Binding an alkyl chain to silicon has been found to result in an interface dipole with a positive pole at the silicon side and a negative pole on the carbon side, due to the higher electronegativity of carbon[68]. In the case of Si-O bonded SAM, there electronegativity difference between the oxygen and Si is increased, resulting in a greater interface dipole.

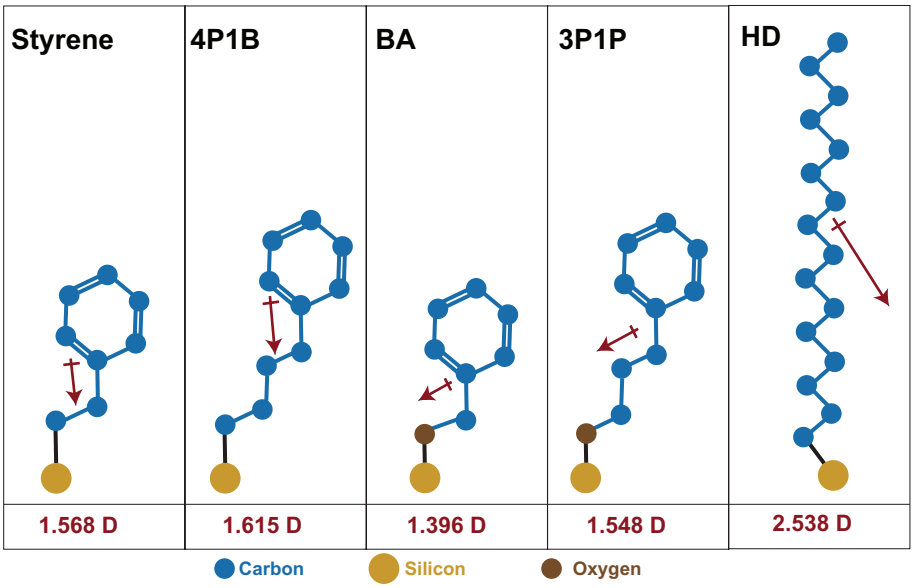


**Fig. 12.** Dipole moments of molecules on Si computed via MOPAC. Arrowhead points to the negative end of the dipole.

In all the measurements, the aromatic SAMs had a lower surface potential than the reference HD SAM. MOPAC computations show that the dipole moments of the aromatic SAMs were lower than the HD molecule (Fig. 12). This is in agreement with our KPFM results. Aromatic SAMs also typically have a greater dielectric constant compared to alkyl SAMs, which would lead a lower surface potential[53]. Si-O bonded SAMs have a lower surface potential than the Si-C SAMs due to the smaller dipole moments. Additionally, under the assumption that the molecules are slightly more tilted as suggested by the WCA and ellipsometry results, the dipole moment would be reduced even more since only the component normal to the surface will be considered. Assuming that Si-O bonded SAMs have a lower packing density compared to Si-C bonded SAMs, this would also result in a larger $A_{SAM,}$ which further lowers the surface potential, consistent with Eq. 1.

*Conductivity Measurements*

One difference when using aromatic SAMs as opposed to aliphatic SAMs is that the conjugation in the phenyl rings provides some degree of conductivity. Several studies have reported the good electrical conductivity of aromatic SAMs[47),53),54)], thus we observed the conductive properties of our SAMs via CAFM. Figure 13 shows the resulting scans and Table III summarizes the results. The CAFM measurements show variations in the scan thus histogram plots rather than line profiles were used to measure the average difference between the aromatic and reference HD regions. Figure 13 shows that the HD SAM regions have very little current passing through it. Due to the short lengths and partial conjugation of the molecules, the aromatic SAMs exhibited much higher current in the CAFM scan. The current passing through the aromatic SAMs ranged from about 9 nA to 64 nA, with the Si-O bonded SAMs exhibiting higher current than Si-C bonded SAMs. The accompanying topographic images during CAFM measurements showed slightly greater topographic contrasts between the aromatic and reference HD SAM compared to that obtained during KPFM measurements. However, the trend is consistent with those obtained via KPFM, as shown in Fig. 14. Note that aromatic SAMs are attached to regions of the substrate which have been lowered by about 1.38 nm due to VUV photolithography and etching (Table II, Fig. 1f).

The larger current passing through the aromatic SAMs can be attributed to the conjugation in the phenyl headgroup. A conjugated system has overlapping π orbitals with delocalized electrons. This increases conductivity of the molecule because the electrons can move around. Aromatic monolayers are known to have superior electrical conductance compared to aliphatic ones[69)]. For short conjugated molecules, the conduction mechanism is believed to be off-resonance tunnelling[70)]. Studies on conjugated molecules have found that charge transport in these systems can occur over a greater distance compared to alkanes. On the other hand, a previous study found that the dominant mechanism of charge transport for alkanethiol SAMs on Au is through-bond tunelling[71)], where current flows along the backbone of the molecule through the overlapping sigma bonds. An alternative possibility is chain-to-chain tunneling or through-space tunneling where charges are able to hop between adjacent hydrocarbon chains. For alkanethiol SAMs, it was found that conductance decreases exponentially as molecule length increases[70)–72)]. Tunnelling rate decreases rapidly with distance thus the conductance of longer alkane chains is very low. This would explain why the HD SAM regions displayed almost no current in our CAFM scans. This would also

explain why 4P1B and 3P1P SAMs have a lower conductivity compared to styrene SAM and BA SAM. Increasing the alkyl chain length increases the tunneling distance, which would result in the decrease of the tunneling current.

One possible explanation why Si-O bonded SAMs exhibited greater currents than the Si-C bonded SAMs is due to the thinner layer of the Si-O SAMs compared to the Si-C SAMs. This allows electrons to pass through with more ease, resulting to a higher current[47]. Also, in a previous study on the transport properties of Si-C and Si-O bonds on alkyl/alkyloxy SAMs on Si (100), Si-O bonded SAMs experienced less length-related damping of the current passing through the monolayers[68]. The Si-O bonded SAMs were also found to have a lower electron effective mass than Si-C bonded ones. Generally, the mobility of free carriers in a material and conductivity are inversely proportional to the carrier effective mass[73], which might explain why our Si-O SAMs exhibited higher currents. However, further studies will be needed to confirm if this relationship is also applicable to aromatic SAMs on n-Si(111). Nevertheless, it is clear that the difference in the interface dipole of the Si-C and Si-O SAMs affected the current transport through the aromatic monolayers.

**Table III.** CAFM and topography contrast of micropatterned SAMs

| | Current (nA) | Topography Contrast (nm) |
|---|---|---|
| Si-C Bonded | | |
| HD – Styrene | 52.3 | -2.03 ± 0.11 |
| HD – 4P1B | 8.9 | -1.98 ± 0.07 |
| Si-O Bonded | | |
| HD – BA | 63.5 | -2.21 ± 0.26 |
| HD – 3P1P | 17.7 | -2.14 ± 1.88 |

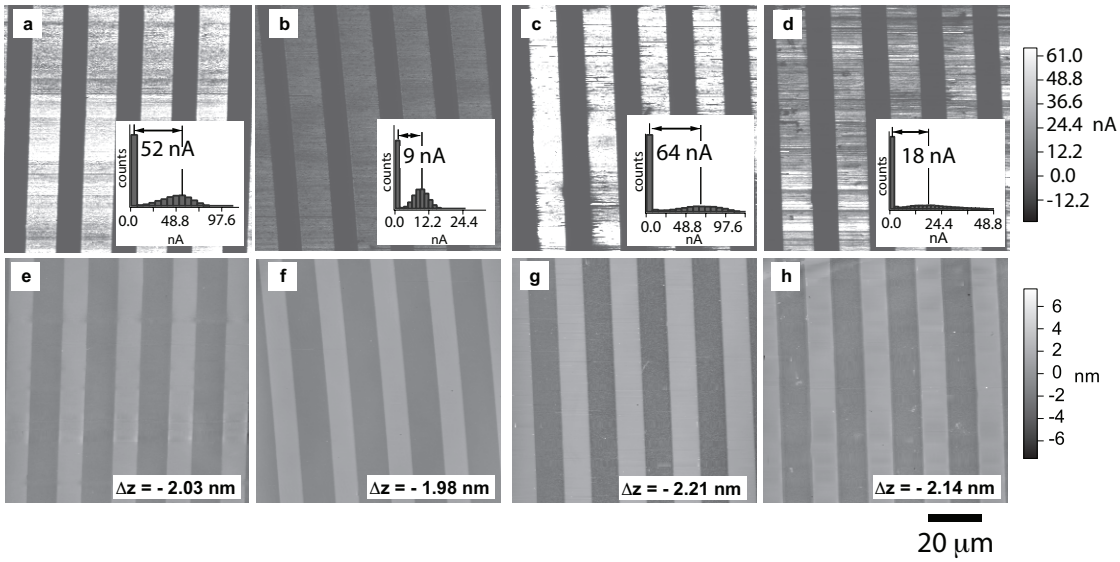


**Fig. 13.** Simultaneously obtained (a-d) CAFM and (e-h) AFM height images of the micropatterned samples, corresponding to (a,e) styrene SAM, (b,f) 4P1B SAM, (c,g) BA SAM, and (d,h) 3P1P SAM. We used HD SAM as a reference at all samples.

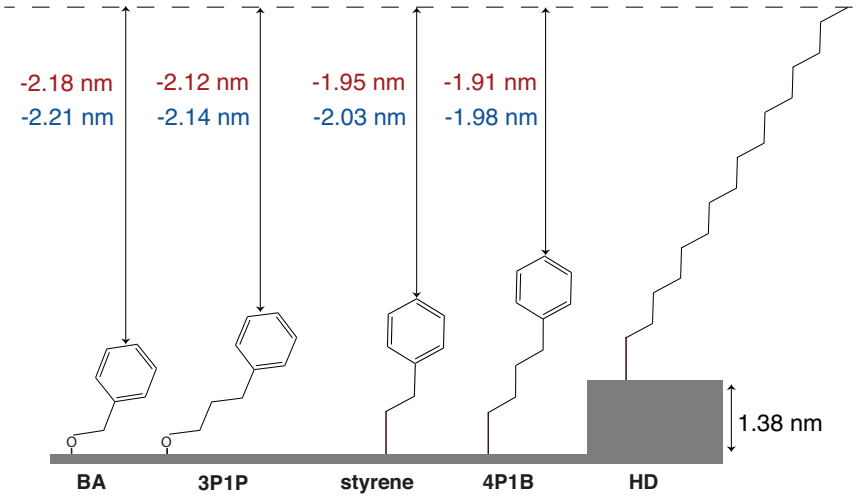


**Fig. 14.** Topography contrast between aromatic SAMs and reference HD SAMs obtained from KPFM (red) and CAFM (blue) measurements

## 4. Conclusions

Our individual characterization of the aromatic SAMs shows that they were organized and densely packed despite the short length of the molecules, possibly due to the π- π stacking of the phenyl rings. XPS results show that the underlying silicon substrate is passivated from oxidation, while WCA and ellipsometry results suggest that Si-O bonded SAMs are tilted more than Si-C bonded SAMs. Estimated dipole moments obtained via

MOPAC show that the molecules experience charge rearrangement upon grafting to the silicon substrate, causing a difference in the intrinsic dipole moment of the precursor molecule and the molecule once it has been grafted to silicon. KPFM measurements found that Si-C bonded SAMs have a higher surface potential than the Si-O bonded SAMs, which agrees with our estimated dipole moments. CAFM results show that the aromatic regions exhibited conductive properties, with Si-O bonded SAMs allowing greater current to pass through compared to Si-C bonded SAMs. Our results suggest that the Si-C and Si-O binding of the SAMs resulted in differences in their molecular packing, net dipole moments, surface potential, and conductivity. Further studies on the band alignment at interfaces and the electronic transport behavior of these SAMs can give us a clearer understanding of how the interface dipole can affect the surface potential/work function and conductivity of these materials.

# References


1) A. Ulman, Chem. Rev. **96**, 1533 (1996).
2) J. J. Gooding, F. Mearns, W. Yang and J. Liu, Electroanalysis **15** [2], 81 (2003).
3) B. D. Booth, S. G. Vilt, J. Ben Lewis, J. L. Rivera, E. A. Buehler, C. McCabe and G. K. Jennings, Langmuir **27**, 5909 (2011).
4) M. Nakano, T. Ishida, H. Sano, H. Sugimura, K. Miyake, Y. Ando and S. Sasaki, Appl. Surf. Sci. **255**, 3040 (2008).
5) M. Behpour and N. Mohammadi, Corros. Sci. **65**, 331 (2012).
6) B. V. Appa Rao, M. Yakub Iqbal and B. Sreedhar, Corros. Sci. **51**, 1441 (2009).
7) T. Wink, S. J. van Zuile, A. Bult and W. P. van Bennekom, Analyst **122**, 43 (1997).
8) H. Lee, W. Lee, J. H. Lee and D. S. Yoon, J. Nanomater. **2016**, 1 (2016).
9) A. Vilan and D. Cahen, Chem. Rev. **117** [5], 4624 (2017).
10) D. K. Aswal, S. Lenfant, D. Guerin, J. V. Yakhmi and D. Vuillaume, Anal. Chim. Acta **568**, 84 (2006).
11) S. Casalini, C. A. Bortolotti, F. Leonardi and F. Biscarini, Chem. Soc. Rev. **46**, 40 (2017).
12) I. H. Campbell, J. D. Kress, R. L. Martin, D. L. Smith, N. N. Barashkov and J. P. Ferraris, Appl. Phys. Lett. **71** [24], 3528 (1997).
13) E. Zojer, T. C. Taucher and O. T. Hofmann, Adv. Mater. Interfaces **6** [14], 1900581 (2019).
14) D. A. Egger, F. Rissner, R. M. Gerold, O. T. Hofmann, L. Wittwer, G. Heimel and E. Zojer, Phys. Chem. Chem. Phys. **12** [17], 4291 (2010).
15) I. Campbell, S. Rubin, T. Zawodzinski, J. Kress, R. Martin, D. Smith, N. Barashkov and J. Ferraris, Phys. Rev. B - Condens. Matter Mater. Phys. **54** [20], 14321 (1996).
16) H. H. Arefi and G. Fagas, J. Phys. Chem. C **118** [26], 14346 (2014).
17) N. Saito, K. Hayashi, H. Sugimura, O. Takai and N. Nakagiri, Chem. Phys. Lett. **349**, 172 (2001).
18) H. Sugimura, K. Hayashi, N. Saito, N. Nakagiri and O. Takai, Appl. Surf. Sci. **188** [3–4], 403 (2002).
19) R. W. Zehner, B. F. Parsons, R. P. Hsung and L. R. Sita, [10], 1121 (1999).
20) P. Tantitarntong, P. Zalar, N. Matsuhisa, K. Nakano, S. Lee, T. Yokota, K. Tajima and T. Someya, ACS Appl. Mater. Interfaces **9** [34], 28151 (2017).
21) C. Ganzorig, K. J. Kwak, K. Yagi and M. Fujihira, Appl. Phys. Lett. **79** [2], 272 (2001).

22) M. C. T. Garcia, T. Utsunomiya, T. Ichii and H. Sugimura, Jpn. J. Appl. Phys. **59** [SD], SDDC06 (2020).
23) A. Szwajca, J. Wei, M. I. Schukfeh and M. Tornow, Surf. Sci. **633**, 53 (2015).
24) A. Natan, N. Kuritz and L. Kronik, Adv. Funct. Mater. **20** [13], 2077 (2010).
25) T. Aqua, H. Cohen, O. Sinai, V. Frydman, T. Bendikov, D. Krepel, O. Hod, L. Kronik and R. Naaman, J. Phys. Chem. C **115** [50], 24888 (2011).
26) G. Heimel, L. Romaner, E. Zojer and J. Bredas, Acc. Chem. Res. **41** [6], 721 (2008).
27) M. D. Porter, T. B. Bright, D. L. Allara and C. E. Chidsey, J. Am. Chem. Soc. **109** [12], 3559 (1987).
28) J. Lu, E. Delamarche, L. Eng, R. Bennewitz, E. Meyer and H. Gu, Langmuir **15**, 8184 (1999).
29) T. Ichii, T. Fukuma, K. Kobayashi, H. Yamada and K. Matsushige, Appl. Surf. Sci. **210**, 99 (2003).
30) A. Natan, Y. Zidon, Y. Shapira and L. Kronik, Phys. Rev. B **73** [193310], 1 (2006).
31) K. Hayashi, N. Saito, H. Sugimura, O. Takai and N. Nakagiri, Ultramicroscopy **91** [1–4], 151 (2002).
32) F. Gao and A. V. Teplyakov, Appl. Surf. Sci. **399**, 375 (2017).
33) Z. Zhang and J. T. Yates, Chem. Rev. **112** [10], 5520 (2012).
34) A. J. Cooper, K. Keyvanfar, A. Deberardinis, L. Pu and J. C. Bean, Appl. Surf. Sci. **257** [14], 6138 (2011).
35) G. Shao, Energy Environ. Mater. **4** [3], 273 (2021).
36) T. He, H. Ding, N. Peor, M. Lu, D. A. Corley, B. Chen, Y. Ofir, Y. Gao, S. Yitzchaik and J. M. Tour, J. Am. Chem. Soc. **130** [5], 1699 (2008).
37) C. Haensch, S. Hoeppener and U. S. Schubert, Chem. Soc. Rev. **39** [6], 2323 (2010).
38) H. Sugimura, A. Hozumi, T. Kameyama and O. Takai, in *Surface and Interface Analysis* (2002).
39) I. G. Hill, C. M. Weinert, L. Kreplak and B. P. van Zyl, Appl. Phys. A **95** [1], 81 (2009).
40) F. Gala and G. Zollo, J. Phys. Chem. C **119** [13], 7264 (2015).
41) J. Veerbeek and J. Huskens, Small Methods **1** [4], 1700072 (2017).
42) H. Sugimura, H. Sano, K.-H. Lee and K. Murase, Jpn. J. Appl. Phys. **45** [6B], 5456 (2006).
43) I. Magid, L. Burstein, O. Seitz, L. Segev, L. Kronik and Y. Rosenwaks, J. Phys. Chem. C **112** [18], 7145 (2008).
44) E. J. Faber, L. C. P. M. De Smet, W. Olthuis, H. Zuilhof, E. J. R. Sudhölter, P. Bergveld

and A. Van Den Berg, ChemPhysChem **6** [10], 2153 (2005).
45) T. Toledano, R. Garrick, O. Sinai, T. Bendikov, A. E. Haj-Yahia, K. Lerman, H. Alon, C. N. Sukenik, A. Vilan, L. Kronik and D. Cahen, J. Electron Spectros. Relat. Phenomena **204**, 149 (2015).
46) M. Hu, F. Liu and J. M. Buriak, ACS Appl. Mater. Interfaces **8** [17], 11091 (2016).
47) Y. Harada, T. Koitaya, K. Mukai, S. Yoshimoto and J. Yoshinobu, J. Phys. Chem. C **117** [15], 7497 (2013).
48) H. Ishii, K. Sugiyama, E. Ito and K. Seki, Adv. Mater. **11** [8], 605 (1999).
49) N. Saito, S. Youda, K. Hayashi, H. Sugimura and O. Takai, Chem. Lett. **31** [12], 1194 (2002).
50) H. Sano, H. Maeda, T. Ichii, K. Murase, K. Noda, K. Matsushige and H. Sugimura, Langmuir **25** [10], 5516 (2009).
51) J. Zhao and K. Uosaki, J. Phys. Chem. B **108** [44], 17129 (2004).
52) M. A. Rampi, O. J. A. Schueller and G. M. Whitesides, Appl. Phys. Lett. **72**, 1781 (1998).
53) T. Toledano, H. Sazan, S. Mukhopadhyay, H. Alon, K. Lerman, T. Bendikov, D. T. Major, C. N. Sukenik, A. Vilan and D. Cahen, Langmuir **30** [45], 13596 (2014).
54) T. Ishida, W. Mizutani, Y. Aya, H. Ogiso, S. Sasaki and H. Tokumoto, J. Phys. Chem. B **106** [23], 5886 (2002).
55) M. C. T. Garcia, T. Utsunomiya, T. Ichii and H. Sugimura, Jpn. J. Appl. Phys. **60** [SE], SE1005 (2021).
56) M. Nonnenmacher, M. P. O'Boyle and H. K. Wickramasinghe, Appl. Phys. Lett. **58** [25], 2921 (1991).
57) H. Sugimura, Y. Ishida, K. Hayashi, O. Takai and N. Nakagiri, Appl. Phys. Lett. **80** [8], 1459 (2002).
58) N. Nakagiri, H. Sugimura, Y. Ishida, K. Hayashi and O. Takai, Surf. Sci. **532**–**535**, 999 (2003).
59) A. I. A. Soliman, T. Ichii, T. Utsunomiya and H. Sugimura, Soft Matter **11** [28], 5678 (2015).
60) H. Sano, H. Maeda, S. Matsuoka, K. H. Lee, K. Murase and H. Sugimura, Jpn. J. Appl. Phys. **47**, 5659 (2008).
61) R. T. W. Popoff, A. A. Zavareh, K. L. Kavanagh and H. Z. Yu, J. Phys. Chem. C **116** [32], 17040 (2012).
62) S.-J. Kim, K. Ryu and S. W. Chang, J. Mater. Sci. **45** [2], 566 (2010).

63) M. J. Stevens, Langmuir **15** [8], 2773 (1999).
64) R. S. Becker, J. A. Golovchenko, E. G. McRae and B. S. Swartzentruber, Phys. Rev. Lett. **55** [19], 2028 (1985).
65) O. Seitz, T. Böcking, A. Salomon, J. J. Gooding and D. Cahen, Langmuir **22** [16], 6915 (2006).
66) H. Sugimura, K. Hayashi and N. Saito, Jpn. J. Appl. Phys. **40**, 4373 (2001).
67) K. Hayashi, N. Saito, H. Sugimura, O. Takai and N. Nakagiri, Langmuir **18** [20], 7469 (2002).
68) F. Thieblemont, O. Seitz, A. Vilan, H. Cohen, E. Salomon, A. Kahn and D. Cahen, Adv. Mater. **20** [20], 3931 (2008).
69) T. Abu-Husein, S. Schuster, D. A. Egger, M. Kind, T. Santowski, A. Wiesner, R. Chiechi, E. Zojer, A. Terfort and M. Zharnikov, Adv. Funct. Mater. **25** [25], 3943 (2015).
70) N. J. Tao, Nanosci. Technol. A Collect. Rev. from Nat. Journals **1**, 173 (2009).
71) W. Wang, T. Lee and A. Reed, Phys. Rev. B - Condens. Matter Mater. Phys. **68** [12], 1 (2003).
72) W. Wang, T. Lee and M. A. Reed, Reports Prog. Phys. **68** [3], 523 (2005).
73) P. P. Edwards, A. Porch, M. O. Jones, D. V. Morgan and R. M. Perks, Dalt. Trans. [19], 2995 (2004).

## Figure Captions

**Fig. 1.** Schematic illustrations for forming the micropatterned SAMs using VUV photolithography

**Fig. 2**. Schematic illustration of photomask used during VUV irradiation

**Fig. 3.** Diagram of the molecules grafted on Si substrate via Si-C and Si-O bonds

**Fig. 4.** XPS spectra of the Si-O and Si-C bonded SAMs obtained from each precursor.

**Fig. 5.** Possible packing arrangements of molecules in SAMs

**Fig. 6**. Ellipsometric thickness of SAMs with MOPAC molecular length of precursors

**Fig. 7.** AFM images of the terrace step structure of (a) styrene SAM, (b) 4P1B SAM, (c) BA SAM and (d) 3P1P SAM

**Fig. 8.** Simultaneously obtained (a-d) surface potential and (e-h) AFM height images of the micropatterned samples, corresponding to (a,e) styrene SAM, (b,f) 4P1B SAM, (c,g) BA SAM, and (d,h) 3P1P SAM. We used HD SAM as a reference for all samples.

**Fig. 9**. AFM images of aromatic SAMs (a-d) and reference HD SAM (e-h) regions of the micropatterned surfaces, corresponding to (a,e) HD-styrene, (b,f) HD-4P1B, (c,g) HD-BA, and (d,h) HD-3P1P. The corresponding HD SAM reference regions (e-h) exhibit damage in the form of etch pits.

**Fig. 10**. Surface potential contrasts of the SAM with respect to reference HD SAM

**Fig. 11.** Dipole moments of precursor molecules computed via MOPAC. Arrowhead points to the negative end of the dipole.

**Fig. 12.** Dipole moments of molecules on Si computed via MOPAC. Arrowhead points to the negative end of the dipole.

**Fig. 13.** Simultaneously obtained (a-d) CAFM and (e-h) AFM height images of the micropatterned samples, corresponding to (a,e) styrene SAM, (b,f) 4P1B SAM, (c,g) BA SAM, and (d,h) 3P1P SAM. We used HD SAM as a reference at all samples.

**Fig. 14.** Topography contrast between aromatic SAMs and reference HD SAMs obtained from KPFM (red) and CAFM (blue) measurements